



# Long-term performance of MgO–SiO<sub>2</sub> binder

Vineet Shah · Milap Dhakal · Allan Scott

Received: 22 June 2021 / Accepted: 1 February 2022 / Published online: 12 February 2022  
© The Author(s) 2022

**Abstract** Magnesium silicate hydrate (M–S–H) formed on reaction of MgO and reactive SiO<sub>2</sub> imparts binding characteristics similar to Portland cement (PC). Limited knowledge is available on the long-term mechanical and durability performance of M–S–H binder systems. In this study, the performance of MgO–SiO<sub>2</sub> binder was assessed up to 365 days. In addition to silica fume (SF), the most widely used silica source with MgO, calcined clay (CC) with kaolinite content of ~ 40–50% and industrial grade metakaolin (MK) were also investigated. Mortar specimens were prepared with all the three silica sources at three different proportion levels of MgO and silica source. Thermodynamic modelling was carried out to further understand the changes occurring in the phase assemblage during hydration for the adopted proportions. Concrete mixes comprising of MgO and MK or SF in a ratio of 1:1 and PC as a control mix were cast a water to binder ratio of 0.4. The compressive strength and porosity were measured at 7, 28, 90 and 365 days on mortar and concrete specimens. In addition, elastic modulus and electrical

resistivity was also measured on the concrete samples at all the above-mentioned ages. MgO mixes with CC and MK showed a continual increase in compressive strength until 365 days whereas strength retrogression was observed in MgO–SF mixes after 90 days. The durability indicators for MgO–MK concrete showed better or similar performance as compared to PC. The aluminum present in the CC and MK helps to improve the overall characteristics of the MgO–SiO<sub>2</sub> binder.

**Keywords** Magnesium oxide · M–S–H · Clay · Compressive strength · Porosity

## 1 Introduction

Magnesium silicate hydrate (M–S–H) is one of the most recently developed and least investigated binders among the various MgO cementitious systems [1] whose current state-of-the-art uses a formulation that is based on the hydration of light burnt MgO in the presence of reactive SiO<sub>2</sub>. The chemical and physical properties of the hydration products are known to change with variations in properties, composition, and proportions of the components [2–6]. However, in the pursuit of an environmentally sustainable alternative to the Portland cement (PC), the dominant binding material for modern day-concrete, M–S–H binders are attracting considerable attention. The M–S–H binder

---

V. Shah (✉) · M. Dhakal · A. Scott  
Department of Civil and Natural Resources Engineering,  
University of Canterbury, Christchurch, New Zealand  
e-mail: vineet.shah9@gmail.com

M. Dhakal  
e-mail: milap.dhakal@pg.canterbury.ac.nz

A. Scott  
e-mail: allan.scott@canterbury.ac.nz



system could have lower carbon footprint as compared to Portland cement due to the lower calcination temperature required to produce reactive MgO and its greater potential to sequester CO<sub>2</sub> [1, 7, 8]. Being a low pH cement, M–S–H cement has found its application as an alternative cementitious material for hazardous waste encapsulation and refractory applications [1, 4, 9, 10]. The compressive strength of MgO–silica paste has been shown to attain satisfactory mechanical properties, chiefly compressive strength. For instance, Zhang et al. [11] were able to formulate a paste with compressive strength as high as 70 MPa at 28 days. Similar encouragement can be identified from the study of Tran and Scott [12] who obtained 28 days strengths as high as 87 MPa in their mortar formulation and Sonat et al. [13] reported strength around 75 MPa in their concrete formulation.

Despite of these encouraging results, one of the major disadvantages of most of the reported M–S–H systems, lies in the selection of silica fume as the source of reactive silica whose cost and limited availability limit potential large scale improvements in sustainability. In addition, the strength gain in MgO–SiO<sub>2</sub> system can be noted to be effected by the curing conditions, especially when cured underwater demonstrating the vulnerability of the system against long term water exposure [13, 14]. In this regard, natural pozzolans that are rich in reactive silica present a more sustainable option for the next generation M–S–H cement formulations due to their natural abundance and minimum processing requirements. Shah and Scott [8, 15, 16] showed clays with even low kaolinite content could be effectively used in combination with MgO to produce a binder. Nevertheless, the properties of M–S–H system thus derived with natural pozzolans require a detailed comparative study with the MgO–SiO<sub>2</sub> system. Furthermore, information on the influence of change in microstructure, in the longer term, due to continued hydration on the durability and transport properties of concrete is unavailable. This study investigates the long-term performance of the M–S–H binder consisting of silica fume, along with widely available kaolinitic clay and metakaolin alongside MgO. The influence of variation in the proportion of MgO and SiO<sub>2</sub> on the binder performance was assessed by measuring the compressive strength, elastic modulus, porosity and electrical resistivity. The influence of reactive alumina present

in clay and metakaolin on the phase assemblage was investigated using thermodynamic modelling.

## 2 Materials

A light-burnt MgO derived from the calcination of magnesium carbonate was used along with silica fume (SF) and metakaolin (MK) supplied by Sika, NZ and BASF, NZ respectively. Kaolinitic clay (CC) with was sourced from the Canterbury region, NZ. The kaolinite content of clay was found to be between 40 and 50%, which was determined using thermogravimetric analysis by measuring the weight loss in the temperature range of 400–800 °C [17]. The clay was calcined at a temperature of 800 °C for 2 h in a muffle furnace prior to use. Golden Bay Cement, NZ, supplied a general-purpose Portland cement (PC) for the study. The oxide composition of raw materials measured using XRF is given in Table 1. The mineralogical composition of the silica sources and MgO was determined using XRD as shown in Fig. 1. Periclase is the major component present in MgO along with an impurity of talc. The presence of brucite peaks indicates pre-hydration of MgO during its storage. The XRD scans of silica fume and metakaolin show the characteristics amorphous region typically observed in pozzolanic materials. Along with subdued amorphous region peaks associated to quartz and muscovite were also observed in the XRD scan of calcined clay. Rounded river gravels with a nominal maximum size of 16 mm were used as coarse aggregate and a river sand was used as fine aggregate in the concrete and mortar mixes. A polycarboxylate ether-based superplasticizer was used to obtain self-compacting concrete mixes with a target flow of 600 ± 50 mm as per ASTM C1611 [18].

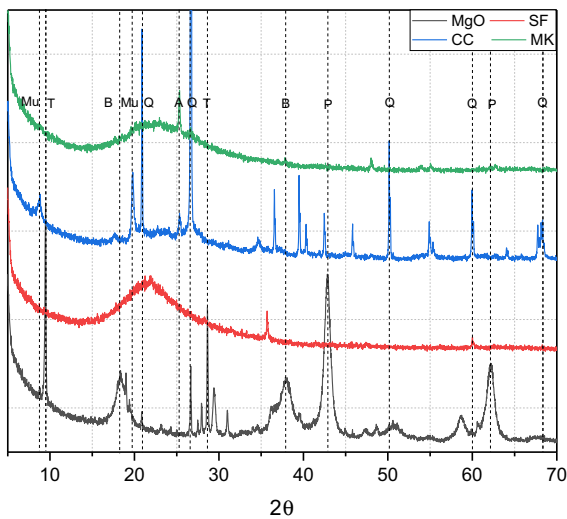
## 3 Methodology

The efficacy of different silica sources on binder performance were first evaluated on mortar specimens for a range of MgO to silica proportion (Table 2). MgO and silica were mixed with sand in a 1:1 ratio (by weight) at a water to binder ratio of 0.4. The raw materials were dry mixed in a Hobart mixer for 2 min before adding water and mixing it for another 5 min. The amount of superplasticizer required to obtain a



**Table 1** Chemical composition (%/100 g) of raw materials

	MgO	Silica fume	Clay	Metakaolin	Cement
CaO	3.6	0.3	0.2	0.01	64.1
SiO <sub>2</sub>	9.1	94.1	60.9	52.7	21.0
Al <sub>2</sub> O <sub>3</sub>	0.4	0.6	24.3	45.2	3.8
MgO	68.3	0.5	0.7	0.03	1.0
Fe <sub>2</sub> O <sub>3</sub>	0.3	0.3	2.1	< 0.01	2.6
SO <sub>3</sub>	0.01	0.05	< 0.01	0.03	2.5
Na <sub>2</sub> O	< 0.01	0.3	0.04	0.2	0.2
K <sub>2</sub> O	0.1	0.8	2.07	0.1	0.5
MnO	–	0.08	0.08	–	0.1
TiO <sub>2</sub>	–	0.01	1.0	0.01	0.3
LOI	17.4	1.9	8.2	0.9	3.3

**Fig. 1** XRD diffractograms of raw materials (Mu: Muscovite, T: Talc, B: Brucite, A: Anatese, Q: Quartz, P: Periclase)

flow of  $150 \pm 10$  mm using a miniature slump test increased with an increase in the proportion of silica in the mixes. Due to the high metakaolin content in MK60 mix, it was difficult to get a homogenous mix even after using superplasticizer. Hence, water to binder ratio of 0.45 as opposed to 0.40 was used to obtain a consistent mix. Cube specimens of  $50 \times 50 \times 50$  mm and cylindrical specimens of 50 mm diameter and 100 mm height were cast using the mortar and placed in an environment-controlled room maintained at a temperature of 20 °C and 60% relative humidity for 24 h. Subsequently, specimens were demolded and placed in a water curing tank maintained at 20 °C until the age of testing. Paste

samples were also cast for SF40, CC40 and MK40 mixes at a water to binder ratio of 0.4 for microstructural analysis.

In addition, concrete specimens were also cast for SF50 and MK50 mix proportion and their properties were compared with conventional PC concrete at the same water to binder ratio of 0.4. The fine aggregate to binder content ratio was 1.25 whereas coarse aggregate to binder content was kept constant at 2 for all the three concrete mixes. The superplasticizer dosage was adjusted among mixes to get a self-compacting concrete. Table 3 summarizes the mix design proportion used for concrete mixes. Cylinders of diameter 100 mm and height 200 mm were cast and cured under water for testing at different ages.

## 4 Experiments

### 4.1 Compressive strength and modulus of elasticity

The compressive strength was measured at 7, 28, 90 and 365 days on the mortar cubes and concrete cylinder specimens at a loading rate of 0.3 MPa/Sec. Elastic modulus of concrete was also measured on the same concrete samples used for compressive strength measurement in accordance with ASTM C469 [19]. The modulus of elasticity was calculated by measuring the slope of stress–strain curve at 40% of the maximum load. Three replicates were tested for all the mixes at each age. Electrical resistance strain gauges (60 mm gauge length) were placed on opposite sides of the cylinder after polishing the surface with

**Table 2** Mix proportion for mortar specimens

	MgO	SF	CC	MK
SF40	0.60	0.40	–	–
SF50	0.50	0.50	–	–
SF60	0.40	0.60	–	–
CC40	0.60	–	0.40	–
CC50	0.50	–	0.50	–
CC60	0.40	–	0.60	–
MK40	0.60	–	–	0.40
MK50	0.50	–	–	0.50
MK60*	0.40	–	–	0.60

\*Due to high metakaolin content the water to binder ratio was increased to 0.45 to maintain similar workability

**Table 3** Mix proportion for concrete mixes by mass

	PC	MgO	Silica fume	Meta-kaolin	Water	Sand	Aggregate	Admixture (% by mass of Binder)
PC	1	–	–	–	0.4	1.25	2	1
SF50	–	0.5	0.5	–	0.4	1.25	2	3
MK50	–	0.5	–	0.5	0.4	1.25	2	5

silicon carbide paper to remove any irregularities. The concrete samples were loaded until failure to measure the compressive strength.

#### 4.2 Porosity and electrical resistivity

The porosity and electrical resistivity of mortar and concrete serves as important durability indicators and helps in understanding the long term potential of the binder system. While porosity of mortar and concrete gives information about the volume of their total permeable voids values of electrical resistivity provide an indication about pore structure and connectivity. The mortar and concrete cylindrical specimens were sliced into 30 mm thick discs for water permeable voids measurement. The disc specimens were dried in an oven maintained at a temperature of 50 °C at least for 7 days or until the time mass of the specimen became constant. After measuring the oven-dried weight, the specimens were saturated with water in vacuum. Subsequently, the saturated and submerged weight of the specimen was measured [20]. For resistivity measurements, the concrete disc specimens used for porosity measurement were dried again in an oven and saturated with 3% saltwater. This was done

in order to minimize the effect of pore solution conductivity between PC and MgO binders. An alternating current with a voltage of 240 mV was applied across the concrete surface and the corresponding current was measured once it stabilized within 60 s. The current values obtained were normalized with respect to the exposed concrete surface area and thickness of the specimen to obtain the resistivity value [4, 10].

#### 4.3 XRD and thermodynamic modelling

XRD was performed on powdered sample to identify different phases formed on hydration. The XRD scan was carried out in the range of 5–70° at a step rate of 0.3 s per step and step size of 0.019° using Rigaku SmartLab installed with Cu K $\alpha$  radiation. Prior to the XRD measurements, the hydration in paste samples was stopped at 7 days using the solvent exchange method, which was subsequently ground to fine powder.

The typical products formed on the hydration of MgO–SiO<sub>2</sub> binder system are brucite and M–S–H. The proportion of these phases formed and the composition of M–S–H formed is affected by initial MgO to SiO<sub>2</sub>



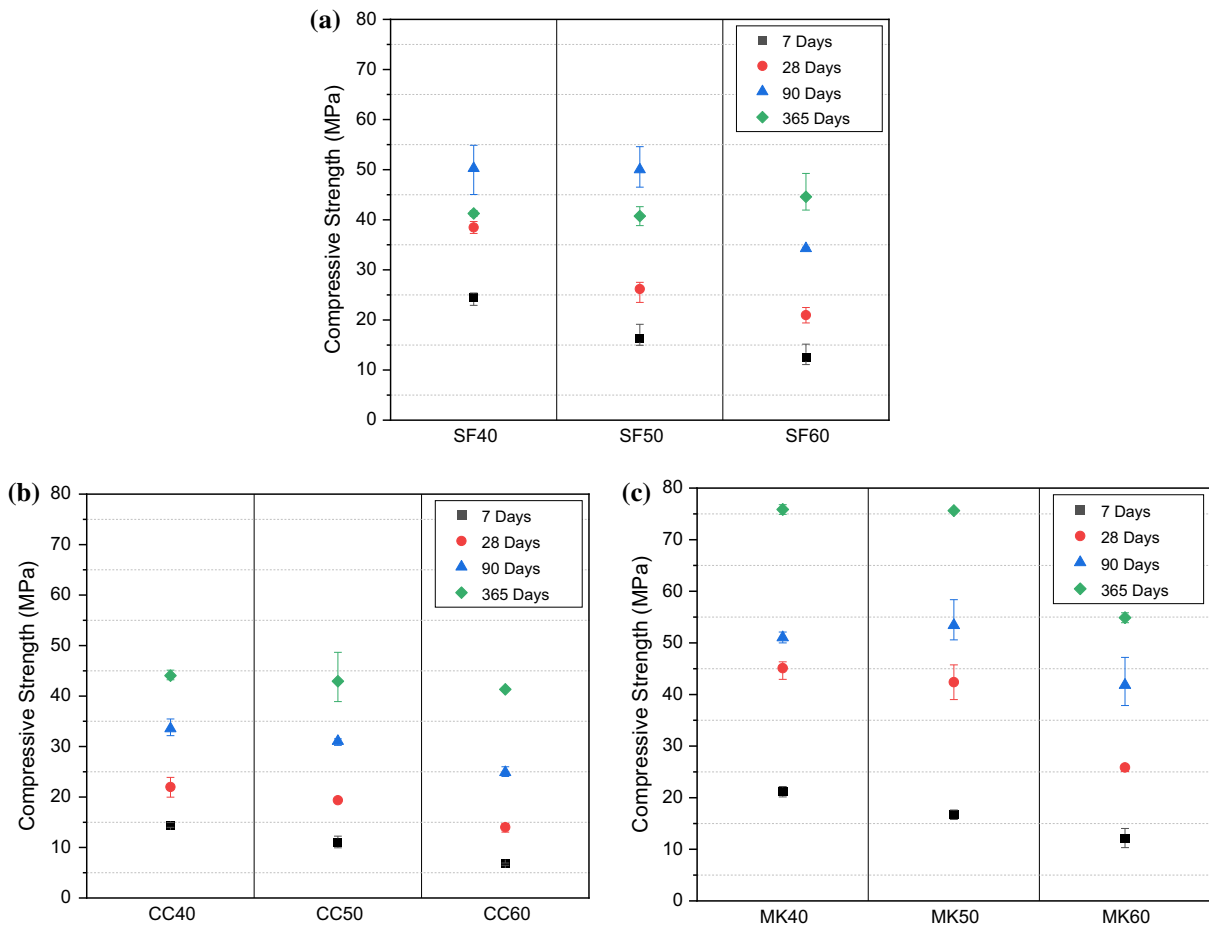


**Fig. 2** Compressive strength of mortar mixes at different ages **a** SF, **b** CC and **c** MK

ratio, which subsequently affects the total solid volume. Thermodynamic modelling is a useful tool that could provide information about phase assemblage of hydrated binder system based on initial chemical composition. Therefore, in this study, GEMS, a geochemical modelling software was used to compute the phase assemblage for all the three silica sources in presence of MgO according to mix proportion given in Table 2 [21, 22]. CEMDATA 18.1 database which includes information on solubility product of M–S–H phase along with other cement hydrates was used to predict equilibrium phase assemblage based on minimization of Gibbs free energy.

## 5 Results and discussion

### 5.1 Mortar compressive strength

Figure 2a shows the effect of difference in the proportion of MgO and SF on compressive strength at different ages. The early age (7 days) compressive strength decreased with an increase in the SF content in the mix. The difference in compressive strength is evident even at 28 days. The higher the MgO content in the mix, the greater is the amount of brucite precipitated during the early ages [23]. The rapid precipitation of brucite in SF40 mix could provide a conducive environment, for the dissolution of SiO<sub>2</sub>, which is dependent on the [OH<sup>-</sup>] [24, 25]. The dissolved silica subsequently reacts with brucite to form M–S–H assisting in further strength

development. Typically, in MgO–SiO<sub>2</sub> binder system, brucite and M–S–H are the primary hydration products, of which the binding characteristics are primarily attributable to the latter [26, 27]. With the progress in hydration, the effect of differences in initial mix proportion decreases with similar compressive strength levels observed for SF40 and SF50 mixes at 90 days. Although an increase in strength is observed for SF60 mix as well from 28 to 90 days, the strength is lower than other two mixes of SF. This could be due to limited availability of magnesium ions in the pore solution to react with all the SF to form M–S–H. The composition of M–S–H formed varies from SF40 to SF60 and may cause difference in the performance characteristics. Li et al. [25] reported the Mg/Si ratio of M–S–H could vary from 0.67 to 1 depending on the initial composition of MgO and SiO<sub>2</sub>. Interestingly, with continued curing from 90 to 365 days, a retrogression in compressive strength was observed for SF40 and SF50 mixes. The dissolution of hydration products and subsequent leaching of ions into the contact water could be the reason for the decline in strength [13, 28]. For the SF60 mix however, an increase in strength was observed during the same period. The contrasting performance could be due to the difference in the hydration products formed. The residual/excess brucite in SF40 mix are likely higher than in the SF60 mix, in addition to a higher Mg/Si of M–S–H due to the higher initial MgO content. The solubility products of brucite and M–S–H (Mg/Si: 1.5) are higher as compared to M–S–H (Mg/Si: 0.75) [29], which could exacerbate the rate of dissolution and diffusion of ions and thus compromising the dimensional stability of the binder. To determine if the leaching of ions create any excess voids, the porosity of samples was also measured at all the ages. The porosity results are discussed in the next section.

Figure 2b and c show the compressive strength MgO–CC and MgO–MK mortar samples. As observed with SF mixes, the compressive strength at early ages decreased with increase in the CC and MK content. In terms of the magnitude, the early age compressive strength of SF and MK mixes were similar whereas the CC mix was somewhat lower. The lower strength of CC mixes could be associated with its lower amorphous silica content as compared to SF and MK. Nevertheless, it is interesting to observe, a low kaolinite content clay could also provide substantial binding properties with MgO. Contrary to the SF

mixes, the strength continued to increase with age for both CC and MK mixes. The 90, strength of CC mixes was still lower than corresponding SF mixes, however, at 365 days, a similar or higher compressive strength was observed. Moreover, little difference in strength values were observed for different MgO and CC proportions at 365 days. An increase in strength in the range of ~ 30–70% was observed from 90 to 365 days for different CC and MK mix proportions. This shows that the MgO–SiO<sub>2</sub> binder system continues to gain strength with time. Along with the formation of M–S–H, the continued increase in strength in CC and MK mixes could also be attributed to the formation of hydrotalcite-like phase, produced on the reaction of reactive alumina present in CC and MK with MgO. The formation of hydrotalcite has been previously reported in MgO systems comprising of slag, fly ash and clay [1, 6, 15, 30]. Hydrotalcite is voluminous in nature and could assist in filling up the empty voids and thereby improve the performance of binder due to an overall reduction in porosity. Jin et al. [30, 31] reported an increase in compressive strength and reduction in shrinkage strain due to the formation of hydrotalcite in MgO activated slag binder. The consistent lower strength of MK60 mix as compared to MK40 and MK50 is due to the difference in water to binder ratio used to prepare the mix. Nonetheless, the continual increase in strength with time shows the efficacy of using MgO alongside metakaolin. Even with higher water content, the compressive strength at 365 days for MK60 was greater than any of the SF or CC mixes.

## 5.2 Volume of permeable voids

Figure 3a shows porosity of the SF mixes at different ages. Minimal difference is observed in the porosity values irrespective of the mix design composition and curing age. The increase in compressive strength with age for SF mixes observed in Fig. 2 does not correlate with the porosity values. This is aberrant compared to conventional binder systems that show a reduction in porosity with an increase in strength and time. One of the reasons for this uncharacteristic behavior could be due to drying shrinkage cracks originated from loss of water from M–S–H. Zhang et al. [32] reported formation of cracks on drying of MgO–SiO<sub>2</sub> mortar samples. Likewise, Shah et al. [33] reported higher drying shrinkage strain for MgO–SF concrete as



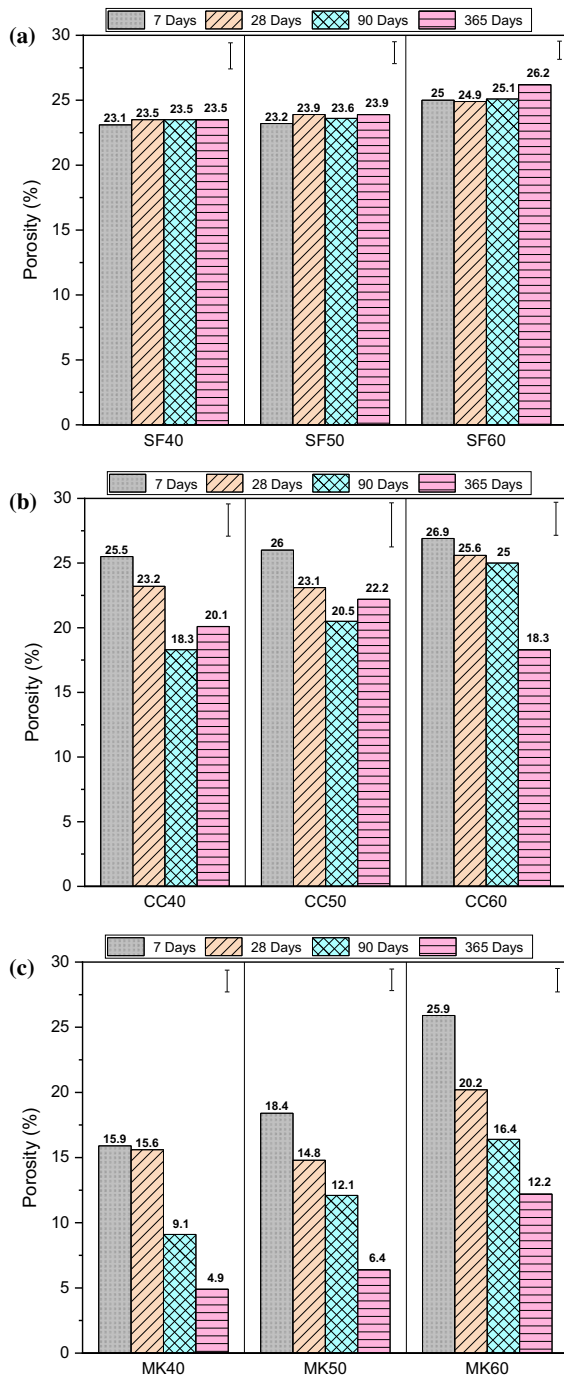


**Fig. 3** Porosity of mortar mixes at different ages **a** SF, **b** CC and **c** MK

compared to PC concrete. In this study, for the porosity measurement, the samples were dried in an oven maintained at 50 °C for at least 7 days. This

preconditioning process could induce changes in the M–S–H formed and overall microstructure of the system. The shrinkage occurring on drying could be negating the effect of evolved pore structure with continued hydration and thus attributing to attain similar porosity values at all ages. The retrogression in strength for SF40 and SF50 mixes from 90 to 365 days, which is postulated due to leaching of ions that could result in an increase in porosity, though this has not been clearly established. The above inferences indicate that the M–S–H formed could be susceptible to dimensional instability in drying environments. Hung et al. also reported similar behavior of negligible change in the porosity of MgO–SiO<sub>2</sub> concrete with time [34].

The CC and MK mixes, showed a reduction in porosity as hydration progresses as illustrated in Fig. 3b and c. Lower porosity was observed for mixes with higher MgO content and substantially lower porosities were noted in the MK mixes, which could be partly credited to the formation of the voluminous hydrotalcite phase that helps in filling up the empty pore space and refinement of pore structure [6, 35]. The overall higher reactive alumina content in MK could lead to the formation of a greater volume of hydrotalcite as compared to CC and hence resulting in lower volume of permeable voids. Shah et al. [33] reported lower drying shrinkage strain for MgO–MK mix as compared to MgO–SF mix in a recent study. The products formed on hydration in CC and MK system are more resistant towards drying, likely due to better stability of M–S–H associated with the incorporation of aluminium resulting in a refined pore structure that inhibits the free movement of ions or water. The reduction in porosity for CC mixes with time supports this idea even though it has overall lower reactive silica content as compared to SF.

For CC40 and CC50 mixes, a slight increase in porosity is observed from 90 to 365 days. This could be attributed due to leaching of magnesium ions from brucite and M–S–H due to prolonged underwater curing. Nevertheless, the porosity is still lower than in SF mixes. Thermodynamic modelling results (discussed in the next section) show the amount of brucite available on complete hydration is higher in CC mixes as compared to SF mixes for all the mix proportions. This suggests that CC mixes could have a higher penchant for dissolution and diffusion of ions, which would result in an increase in porosity and reduction in

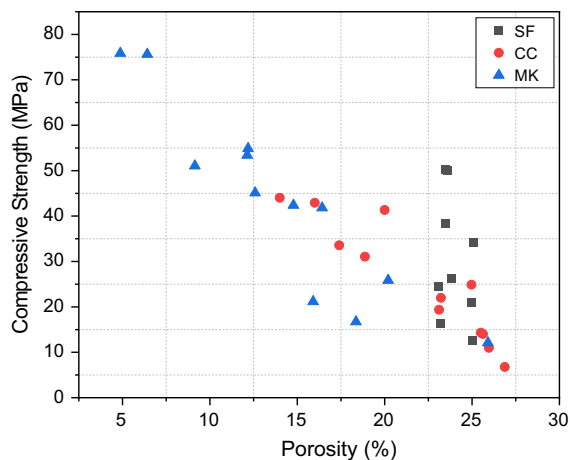


**Fig. 4** Comparison of porosity and compressive strength of all the SF, CC and MK mortar mixes

strength. However, it is not quite observed from the porosity and compressive strength data indicating the hydration phases formed in MgO–SiO<sub>2</sub> binder in the presence of aluminium could provide better performance characteristics. Figure 4 compares the compressive strength and porosity of all three silica sources. A linear trend is observed for CC and MK mixes, with an increase in the compressive strength a reduction in porosity is observed while for SF mixes at same porosity level a range of compressive strength is observed. Dhakal et al. [36] also reported a similar trend between strength and porosity for a range of MgO–MK mixes.

### 5.3 Phase assemblage from XRD and thermodynamic modelling

The phase assemblage of the products formed on hydration in different mixes was qualitatively analyzed using XRD. Figure 5 compares the XRD scans of 7 days hydrated SF40, CC40 and MK40 mixes. Peaks corresponding to brucite and unreacted periclase are observed in all the three mixes whilst hydrotalcite peaks are only observed in CC40 and MK40 mixes. The presence of reactive alumina in CC and MK is speculated to aid in the formation of hydrotalcite. The peaks corresponding to M–S–H are not distinctly visible due to its poor crystalline nature. However, the presence of the broad regions (35–37°,

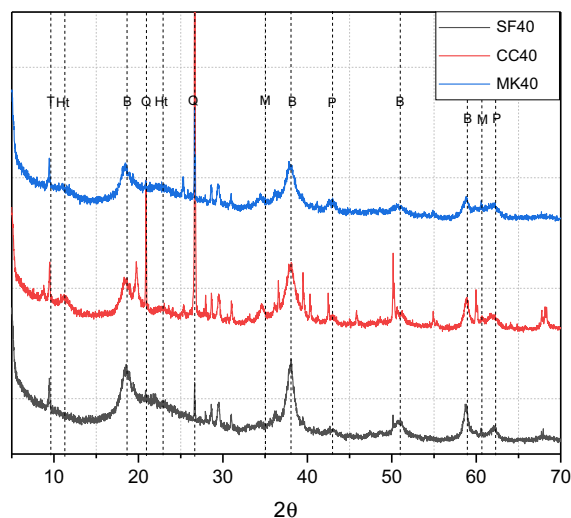


**Fig. 5** XRD scans of 7 days hydrated paste samples (T: Talc, Ht: Hydrotalcite, B: Brucite, Q: Quartz, M: M–S–H, P: Periclase)

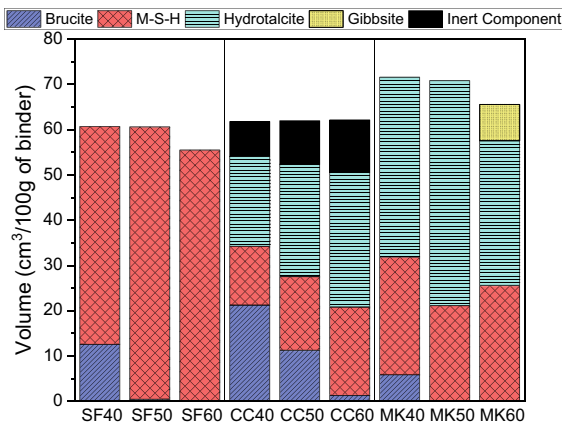
59–62°) in all the three mixes indicates its formation as described in the literature [5, 37].

Pure phase compositions were considered in the model to explicitly understand the influence of the difference in the mix proportion on phase assemblage. A pure metakaolin has a composition of 2SiO<sub>2</sub>·Al<sub>2</sub>O<sub>3</sub>. Depending on the mix proportion, the corresponding amount of SiO<sub>2</sub> and Al<sub>2</sub>O<sub>3</sub> was calculated and used as input in the model. Since the CC used in the study had a kaolinite content between 40 and 50%, to replicate a similar effect in the thermodynamic modelling calculations, it was assumed that only 50% of the total available SiO<sub>2</sub> and Al<sub>2</sub>O<sub>3</sub> in metakaolin phase was reactive while the remaining 50% metakaolin was treated as an inert component. Table 4 summarizes the initial bulk chemical composition used to compute the phase assemblage.

Figure 6 shows the solid phase volume of hydration products for all the three silica sources. Brucite and M–S–H are the major hydrates predicted in all the three silica sources. The M–S–H phase illustrated here is a solid solution between M–S–H having Mg/Si ratio of 1.5 and 0.75. In CC and MK blends, in addition to brucite and M–S–H phase, the formation of hydrotalcite is predicted, due to the presence of aluminum. The phase predictions from thermodynamic calculations are consistent with the XRD results obtained (Fig. 5). For SF mixes, with an increase in the silica proportion

**Table 4** Bulk composition used for prediction of phase assemblage

	MgO	SiO <sub>2</sub>	Al <sub>2</sub> O <sub>3</sub>
SF40	60	40	–
SF50	50	50	–
SF60	40	60	–
CC40	60	10.8	9.2
CC50	50	13.5	11.5
CC60	40	16.2	13.8
MK40	60	21.6	18.4
MK50	50	27.0	23.0
MK60	40	32.4	27.6

**Fig. 6** Phase assemblage prediction from thermodynamic modelling

of the binder, the amount of residual brucite available reduces, indicating conversion of MgO to M–S–H and the proportion of M–S–H phase with lower Mg/Si ratio increases. It is interesting to note that the total solid volume of the hydrates either remains the same or reduces with an increase in the SF content. Formation of lower Mg/Si ratio M–S–H ( $\rho = 2.35 \text{ g/cm}^3$ ), which is a denser phase as compared to M–S–H with Mg/Si ratio of 1.5 ( $\rho = 2.25 \text{ g/cm}^3$ ) [38] could be the reason associated with it. This implies, in actual system, SF40 mix composition on complete hydration would have higher space-filling capacity, which will eventually result in overall lower pore volume. However, from the porosity results in Fig. 3, no distinct difference was observed between porosity of different SF mixes. In CC and MK mix composition, the total solid volume also reduces with an increase in their content;

however, the volume is greater than the corresponding SF mixes particularly for the MK mixes. The modelled values are in agreement with the experimental results, where a lower porosity for CC and MK mortar mixes is observed as compared to SF mixes. Thermodynamic modelling suggests hydrotalcite as the predominant phase formed on hydration in CC and MK blends. Hydrotalcite is voluminous in nature ( $\rho = 2.01 \text{ g/cm}^3$ ) [39] and hence could offer higher space-filling capacity as compared to M–S–H. Studies have demonstrated the formation of hydrotalcite like phase in binders comprising of MgO and aluminosilicates [6, 16, 30, 35, 40]. The notion is further supported by the presence of XRD peaks corresponding to hydrotalcite in hydrated CC40 and MK40 mixes.

Moreover, the aluminum, present in CC and MK, could also be incorporated into the M–S–H phase, similar to the incorporation of aluminum in C–S–H in PC binders. This could subsequently alter the properties of the M–S–H formed and may limit the amount of aluminum available for formation of hydrotalcite. Recent studies from Bernard et al. [41] and Shah et al. [6] confirmed incorporation of aluminum can occur in M–S–H. It was not possible to model the effect of aluminium inclusion/substitution in M–S–H in thermodynamic calculations performed since the solubility data corresponding to it is unavailable. Nevertheless, it helps in establishing the fact the hydrotalcite and M–S–H could coexist simultaneously.

The thermodynamic modelling prediction shows the presence of excess brucite in the case of the SF40 mix which may be associated with the strength retrogression observed for SF40 mortar samples from 90 to 365 days. On prolonged curing, the excess brucite present in the system might leach out, resulting in creation of additional void space and a consequent reduction in strength. A similar reduction in strength was also observed for SF50 mix from 90 to 365 days, although thermodynamically the amount of brucite predicted on complete hydration is limited. For the SF60 mix, however an increase in strength was observed during the same period. In spite of having similar porosity and negligible brucite content, the difference in behavior of SF50 and SF60 mix is intriguing. This suggests that other than brucite leaching out of the system some other factor is also influencing the performance of the binder. Thermodynamic modelling results suggests M–S–H as the

only hydration product in both the mix proportions, but with different composition. The higher Mg/Si ratio in SF50 mix might leach out some of the magnesium ions eventually resulting in the strength loss. For CC mixes, a higher amount of brucite is predicted at all the proportions as compared to SF mixes. Moreover, even for CC60 mix, the M–S–H formed has a higher Mg/Si ratio. As opposed to SF mixes, an increase in strength was observed from 90 to 365 days for all the CC mixes. Two reasons could be hypothesized for this: 1) Incorporation of Al in the M–S–H is assisting in inducing greater stability to M–S–H structure thereby limiting the leaching of magnesium ions from it, 2) The voluminous nature of hydrotalcite could lead to a refinement of the pore structure along with a reduction in porosity, which impedes the movement of ions. The overall higher aluminum content in the MK content could lead to higher incorporation in M–S–H and along with formation of higher amounts of hydrotalcite (evident from thermodynamic modelling results). The validity of the hypothesis suggested needs further investigation to be confirmed, however, the results from the concrete specimens, discussed in the next section, provides some additional insights on these perspectives.

#### 5.4 Concrete mechanical properties

The range of tests conducted on mortar specimens alongside thermodynamic modelling gives an indication of the performance characteristics for different silica sources and their proportion in the binder. Although tests on mortar specimens provide an indication of likely binder performance, to make certain its potential applicability as a construction material, it is important to investigate the performance of concrete directly. The SF50 and MK50 concrete mixes were investigated and compared with PC at similar water to binder ratio. Figure 7 shows the compressive strength of concrete mixes examined from 7 to 365 days. The compressive strength of PC mix is consistently greater than SF50 and MK50 mixes at all ages. The increase in strength of PC mix is minimal beyond 90 days, however, an increase of approximately 40% was observed for MK50 mix, which is consistent with the mortar results. The gap between the compressive strength of PC and MK mix narrowed from approximately 40 to only 14%, while for the SF50 mix, no strength gain was observed

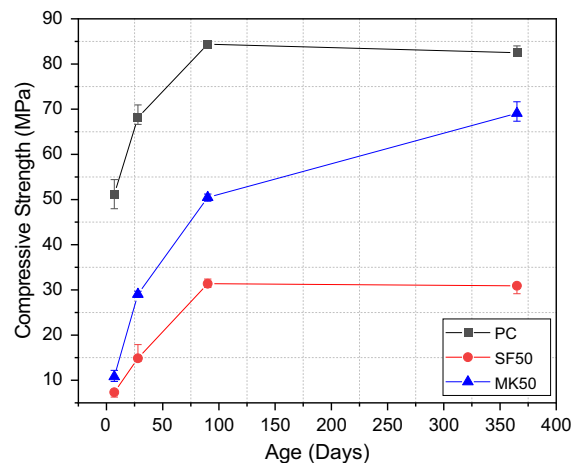


**Fig. 7** Compressive strength of concrete mixes at 7, 28, 90 and 365 days

beyond 90 days. A slight reduction in strength was observed for the SF50 mix; however, it was not as prominent as was observed in the mortar samples. The 365 days compressive strength of SF50 mix was lower by approximately 133 and 173% as compared to MK50 and PC mix.

The elastic modulus of concrete mixes at different ages is shown in Fig. 8. A distinct difference is observed between the elastic modulus of MgO concrete mixes and PC mix. The modulus of elasticity of PC increases from 7 to 28 days, thereafter, the variation in the value is minimal. In the case of SF50, the elastic modulus increased with age until 90 days, however, afterward a reduction in elastic modulus value was observed. Retrogression of compressive

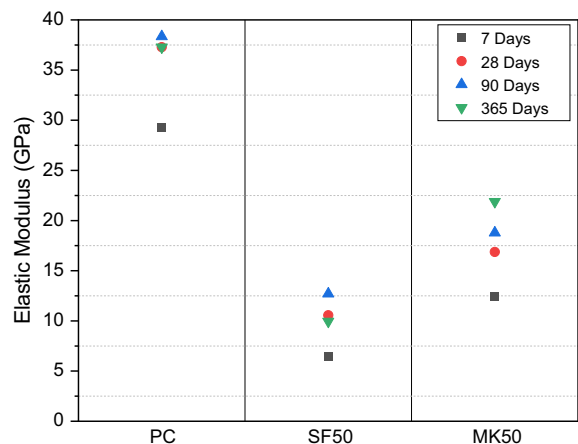


**Fig. 8** Elastic modulus of PC, SF50 and MK50 concrete mixes

strength on prolonged curing could be the reason for reduction in elastic modulus value at 365 days. Hung et al. [34] also reported elastic modulus value in a similar range for MgO–SiO<sub>2</sub> binder. For the MK50 mix, a continual increase in elastic modulus was observed with age, with the value reaching approximately 23 GPa at 365 days. The elastic modulus of concrete is governed by numerous factors ranging from binder type, water to cement ratio, aggregate content, curing age and regime [42, 43]. In this study, all the parameters other than the binder were held constant. This points out the deviation observed in the elastic modulus between concrete mixes is primarily because of the binder and hydration products formed. The higher and stable value of elastic modulus of MK50 mix as compared to SF50 mix indicates the hydration products formed in MK50 mix could possess superior properties that aid in providing better mechanical and stiffness characteristics. Hay et al. [44] demonstrated incorporation of aluminum in C–S–H, the major hydration product in PC, led to an increase in the elastic modulus and mechanical properties of the phase due to enhanced cross-linking and improved compactibility. An analogous result of the incorporation of aluminum in M–S–H could lead to an improvement of MgO binder performance containing MK.

### 5.5 Concrete durability indicators

The nature of the hydration products formed also dictates the durability behaviour of the concrete along with the mechanical properties. A comparison of the two major durability indicators: porosity and electrical resistivity were made in this investigation. Figure 9 shows the measured porosity and resistivity of all three concrete mixes at different ages. The porosity of SF50 concrete mix did not vary with time, and shows similar behaviour to the SF mortar mixes (Fig. 3). While for PC and MK50 mixes, a reduction in porosity was observed with age, with almost similar values at 365 days. This implies that the space-filling capacity of the products formed in MK50 are comparable to PC. However, a notable difference was observed in the electrical resistivity between the mixes. The resistivity of MK50 mix was greater than PC mix at all ages. In addition, an increase of approximately 200 and 350% is observed at 28 and 90 days respectively from 7 days in MK50 mix whereas the change was minimal from 7

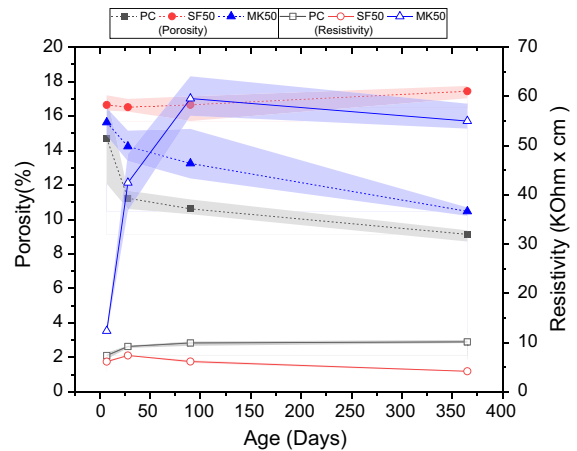


**Fig. 9** Porosity and electrical resistivity of PC, SF50 and MK50 concrete mixes at different age

to 90 days for PC mix. The increase in resistivity value could be associated with an evolving physical structure. The electrical resistivity of concrete provides information about the pore connectivity of the concrete [45]. The high resistivity value of MK50 suggests presence of intricate pore structure with high tortuosity. The formation of hydrotalcite could be the key factor for the development dense microstructure with refined pores that inhibit or slow down the flow of ions. In a recent study, Shah et al. [35] demonstrated a denser and refined microstructure for MgO–MK mix as compared to MgO–SF or PC mixes. From the standpoint of ingress of ions from an external source in concrete, such system could provide an efficient solution. Similar traits of high electrical resistivity has been reported for PC concrete comprising of calcined clay or metakaolin [46, 47]. The low resistivity of the SF50 mix could be attributed to higher porosity and cracks originating from drying, which provide an easy path for the movement of ions.

The study showed the possibility of using calcined clay alongside MgO in terms of both mechanical durability properties. The concrete properties of MK50 compared to the PC mix provides a compelling reason for further investigations, which could result in use a low carbon binder construction material.

## 6 Conclusions

In this study, the performance of MgO–SiO<sub>2</sub> binder with three different silica sources was evaluated. The

effect of variation of MgO to SiO<sub>2</sub> proportion on binder performance in terms of mechanical and durability properties was investigated. The major findings from the study are as follows:

- The compressive strength at an early age (7 days) is influenced by the MgO–SiO<sub>2</sub> ratio. A reduction in compressive strength was observed with a decrease in the MgO content of the binder irrespective of the silica source.
- Continuous improvement in strength was observed as hydration progress for calcined clay and metakaolin mixes up to 365 days, whereas retrogression in compressive strength was observed from 90 to 365 days.
- The porosity of SF mixes was found to be unaffected by the binder composition and curing age. Excessive cracking due to drying was suggested as the plausible cause.
- Thermodynamic modelling prediction showed the formation of hydrotalcite-like phase in CC and MK mixes along with M–S–H and brucite. The voluminous nature of hydrotalcite aided in improving the mechanical performance and reducing the porosity.
- The elastic modulus of MgO concrete mixes was lower than PC. However, MgO–MK mix showed significantly better performance as compared to MgO–SF mix. As compared to PC, the MgO–MK mix showed similar compressive strength and better pore structure characteristics.

**Acknowledgements** The authors would like to acknowledge the financial support provided by the Ministry of Business, Innovation and Employment, New Zealand for this project

**Funding** Open Access funding enabled and organized by CAUL and its Member Institutions.

**Data Availability** Some or all data, models, or code that support the findings of this study are available from the corresponding author upon reasonable request.

#### Declarations

**Conflict of interest** The authors declare that they have no conflict of interest.

**Open Access** This article is licensed under a Creative Commons Attribution 4.0 International License, which permits use, sharing, adaptation, distribution and reproduction in any medium or format, as long as you give appropriate credit to the

original author(s) and the source, provide a link to the Creative Commons licence, and indicate if changes were made. The images or other third party material in this article are included in the article's Creative Commons licence, unless indicated otherwise in a credit line to the material. If material is not included in the article's Creative Commons licence and your intended use is not permitted by statutory regulation or exceeds the permitted use, you will need to obtain permission directly from the copyright holder. To view a copy of this licence, visit <http://creativecommons.org/licenses/by/4.0/>.

#### References

1. Walling SA, Provis JL (2016) Magnesia-based cements: a journey of 150 years, and cements for the future? *Chem Rev* 116:4170–4204. <https://doi.org/10.1021/acs.chemrev.5b00463>
2. Kalousek GL, Mui D (1954) Studies on formation and recrystallization of intermediate reaction products in the system magnesia-silica-water. *J Am Ceram Soc* 37:38–42. <https://doi.org/10.1111/j.1151-2916.1954.tb14001.x>
3. Brew DRM, Glasser FP (2005) Synthesis and characterisation of magnesium silicate hydrate gels. *Cem Concr Res* 35:85–98. <https://doi.org/10.1016/j.cemconres.2004.06.022>
4. Jin F, Al-Tabbaa A (2014) Strength and hydration products of reactive MgO–silica pastes. *Cem Concr Compos* 52:27–33. <https://doi.org/10.1016/j.cemconcomp.2014.04.003>
5. Tonelli M, Martini F, Calucci L et al (2016) Structural characterization of magnesium silicate hydrate: towards the design of eco-sustainable cements. *Dalton Trans* 45:3294–3304. <https://doi.org/10.1039/c5dt03545g>
6. Shah V, Scott A (2021) Hydration and microstructure characteristics of MgO in presence of metakaolin and silica fume. *Cem Concr Compos* 121:104068
7. Al-Tabbaa A (2013) Reactive magnesia cement. In: *Eco-efficient concrete*, Elsevier Ltd, pp 523–543
8. Shah V, Scott A (2021) Use of kaolinite clays in development of a low carbon MgO-clay binder system. *Cem Concr Res* 144:106422. <https://doi.org/10.1016/j.cemconres.2021.106422>
9. Zhang T, Cheeseman CR, Vandeperre LJ (2011) Development of low pH cement systems forming magnesium silicate hydrate (M-S-H). *Cem Concr Res* 41:439–442. <https://doi.org/10.1016/j.cemconres.2011.01.016>
10. Zhang T, Vandeperre LJ, Cheeseman CR (2012) Magnesium-silicate-hydrate cements for encapsulating problematic aluminium containing wastes. *J Sustain Cem Based Mater* 1:34–45. <https://doi.org/10.1080/21650373.2012.727322>
11. Zhang T, Vandeperre LJ, Cheeseman CR (2014) Formation of magnesium silicate hydrate (M-S-H) cement pastes using sodium hexametaphosphate. *Cem Concr Res* 65:8–14. <https://doi.org/10.1016/j.cemconres.2014.07.001>
12. Tran HM, Scott A (2017) Strength and workability of magnesium silicate hydrate binder systems. *Constr Build Mater* 131:526–535. <https://doi.org/10.1016/j.conbuildmat.2016.11.109>



13. Sonat C, Teo WW, Unluer C (2018) Performance and microstructure of MgO-SiO<sub>2</sub> concrete under different environments. *Constr Build Mater* 184:549–564. <https://doi.org/10.1016/j.conbuildmat.2018.07.032>
14. Tran H (2019) Development of magnesium silicate hydrate binder systems. University of Canterbury
15. Shah V, Scott A (2019) Use of Kaolin clay as a source of silica in MgO-SiO<sub>2</sub> binder. In: Third international conference on calcined clays for sustainable concrete. New Delhi
16. Shah V, Scott A (2019) Hydration study of ternary magnesium-silicate-carbonate system. In: Concrete institute of Australia's biennial national conference. Sydney, pp 3–9
17. Krishnan S, Emmanuel AC, Shah V, et al (2018) Industrial production of limestone calcined clay cement: experience and insights. *Green Mater* 1–14
18. ASTM C1611 (2021) Standard test method for slump flow of self-consolidating concrete
19. ASTM C469 (2014) Standard test method for static modulus of elasticity and Poisson's ratio of concrete in compression. ASTM International. pp 1–5 <https://doi.org/10.1520/C0469>
20. Alexander MJ (2005) Durability indexes and their use in concrete engineering. In: International RILEM symposium on concrete science and engineering: tribute to Arnon Bentur. Evanston, pp 9–22
21. Kulik DA, Wagner T, Dmytrieva SV et al (2013) GEM-Selektor geochemical modeling package: revised algorithm and GEMS3K numerical kernel for coupled simulation codes. *Comput Geosci* 17:1–24. <https://doi.org/10.1007/s10596-012-9310-6>
22. Damidot D, Lothenbach B, Herfort D, Glasser FP (2011) Thermodynamics and cement science. *Cem Concr Res* 41:679–695. <https://doi.org/10.1016/j.cemconres.2011.03.018>
23. Li Z, Xu Y, Zhang T et al (2018) Effect of MgO calcination temperature on the reaction products and kinetics of MgO-SiO<sub>2</sub>-H<sub>2</sub>O system. *J Am Ceram Soc* 61:252–259. <https://doi.org/10.1111/jace.16201>
24. Niibori Y, Chida T, Tochiyama O (2000) Dissolution rates of amorphous silica in highly alkaline solution. *J Nucl Sci Technol* 37:349–357. <https://doi.org/10.1080/18811248.2000.9714905>
25. Li Z, Zhang T, Hu J et al (2014) Characterization of reaction products and reaction process of MgO-SiO<sub>2</sub>-H<sub>2</sub>O system at room temperature. *Constr Build Mater* 61:252–259
26. Gartner E, Sui T (2018) Alternative cement clinkers. *Cem Concr Res* 114:27–39. <https://doi.org/10.1016/j.cemconres.2017.02.002>
27. Kuenzel C, Zhang F, Ferrándiz-Mas V et al (2018) The mechanism of hydration of MgO-hydromagnesite blends. *Cem Concr Res* 103:123–129. <https://doi.org/10.1016/j.cemconres.2017.10.003>
28. Jin F, Al-Tabbaa A (2014) Strength and hydration products of reactive MgO-silica pastes. *Cement Concr Compos* 52:27–33. <https://doi.org/10.1016/j.cemconcomp.2014.04.003>
29. Nied D, Enemark-Rasmussen K, L'Hopital E et al (2016) Properties of magnesium silicate hydrates (M-S-H). *Cem Concr Res* 79:323–332. <https://doi.org/10.1016/j.cemconres.2015.10.003>
30. Jin F, Gu K, Al-Tabbaa A (2015) Strength and hydration properties of reactive MgO-activated ground granulated blastfurnace slag paste. *Cement Concr Compos* 57:8–16. <https://doi.org/10.1016/j.cemconcomp.2014.10.007>
31. Jin F, Gu K, Al-Tabbaa A (2014) Strength and drying shrinkage of reactive MgO modified alkali-activated slag paste. *Constr Build Mater* 51:395–404. <https://doi.org/10.1016/j.conbuildmat.2013.10.081>
32. Zhang T, Liang X, Li C et al (2016) Control of drying shrinkage in magnesium silicate hydrate (m-s-h) gel mortars. *Cem Concr Res* 88:36–42. <https://doi.org/10.1016/j.cemconres.2016.05.011>
33. Shah V, Scott A (2021) Assessment of the hardened concrete properties of MgO-SiO<sub>2</sub> binder. *ACI Mater J* 118:223–232
34. Tran H, Scott A, Dhakal R (2019) Mechanical and durability properties of concrete with magnesium silicate hydrate binder systems. *Mag Concr Res* 72(13):1–31. <https://doi.org/10.1680/jmacr.18.00217>
35. Shah V, Dhandapani Y, Scott A (2021) Pore structure characteristics of MgO-SiO<sub>2</sub> binder (Accepted-In Press). *J Am Ceram Soc*. <https://doi.org/10.1111/jace.17971>
36. Dhakal M, Scott AN, Shah V et al (2021) Development of a MgO-metakaolin binder system. *Constr Build Mater* 284:122736. <https://doi.org/10.1016/j.conbuildmat.2021.122736>
37. Zhang T, Zou J, Wang B et al (2018) Characterization of magnesium silicate hydrate (MSH) gel formed by reacting MgO and silica fume. *Materials* 11:1–15. <https://doi.org/10.3390/ma11060909>
38. Bernard E, Lothenbach B, Chlique C et al (2019) Characterization of magnesium silicate hydrate (M-S-H). *Cem Concr Res* 116:309–330. <https://doi.org/10.1016/j.cemconres.2018.09.007>
39. Balonis M, Glasser FP (2009) The density of cement phases. *Cem Concr Res* 39:733–739. <https://doi.org/10.1016/j.cemconres.2009.06.005>
40. Abdel-Gawwad HA, Abd El-Aleem S, Amer AA et al (2018) Combined impact of silicate-amorphicity and MgO-reactivity on the performance of Mg-silicate cement. *Constr Build Mater* 189:78–85. <https://doi.org/10.1016/j.conbuildmat.2018.08.171>
41. Bernard E, Lothenbach B, Pochard I, Rentsch D (2020) Aluminum incorporation into magnesium silicate hydrate (M-S-H). *Cem Concr Res* 128:105931. <https://doi.org/10.1016/j.cemconres.2019.105931>
42. Mehta PK, Monteiro PJM (2006) Concrete microstructure, properties, and materials, 4th edn. McGraw-Hill education, New York
43. Neville AM (2011) Properties of concrete, 5th edn. Prentice Hall, Malaysia
44. Hay R, Li J, Celik K (2020) Influencing factors on micromechanical properties of calcium (aluminio) silicate hydrate C-(A-)S-H under nanoindentation experiment. *Cem Concr Res* 134:106088. <https://doi.org/10.1016/j.cemconres.2020.106088>
45. Dhandapani Y, Santhanam M (2017) Assessment of pore structure evolution in the limestone calcined clay cementitious system and its implications for performance. *Cem Concr Compos* 84:36–47. <https://doi.org/10.1016/j.cemconcomp.2017.08.012>
46. Dhandapani Y, Santhanam M (2020) Investigation on the microstructure-related characteristics to elucidate

performance of composite cement with limestone-calcined clay combination. Cem Concr Res 129:105959. <https://doi.org/10.1016/j.cemconres.2019.105959>

47. Ghoddousi P, Adelzade Saadabadi L (2017) Study on hydration products by electrical resistivity for self-compacting concrete with silica fume and metakaolin. Constr

Build Mater 154:219–228. <https://doi.org/10.1016/j.conbuildmat.2017.07.178>

**Publisher's Note** Springer Nature remains neutral with regard to jurisdictional claims in published maps and institutional affiliations.

